POLITECNICO DI TORINO
Repository ISTITUZIONALE

Physics Informed Neural Network for Continuous and Cuffless Arterial Blood Pressure

Original
Physics Informed Neural Network for Continuous and Cuffless Arterial Blood Pressure / Delrio, F., Randazzo, V., Cirrincione, G., Pasero, E.. - ELETTRONICO. - (2025), pp. 143-148. (2025 IEEE International Conference on Artificial Intelligence for Learning and Optimization (ICoAILO) Bali (Idn) 07-09 August 2025) [10.1109/icoailo66760.2025.11156047].

Availability:
This version is available at: 11583/3003672 since: 2025-10-29T10:36:05Z

Publisher:
IEEE

Published
DOI:10.1109/icoailo66760.2025.11156047

Terms of use:

This article is made available under terms and conditions as specified in the corresponding bibliographic description in the repository

Publisher copyright
IEEE postprint/Author's Accepted Manuscript

©2025 IEEE. Personal use of this material is permitted. Permission from IEEE must be obtained for all other uses, in any current or future media, including reprinting/republishing this material for advertising or promotional purposes, creating new collecting works, for resale or lists, or reuse of any copyrighted component of this work in other works.

(Article begins on next page)

19 November 2026

Physics Informed Neural Network for Continuous and Cuffless Arterial Blood Pressure

Federico Delrio
DET
Politecnico di Torino
Turin, Italy
federico.delrio@polito.it

Vincenzo Randazzo
DET
Politecnico di Torino
Turin, Italy
vincenzo.randazzo@polito.it

Giansalvo Cirrincione
lab. LTI
University of Picardie Jules Verne
Amiens, France
exin@u-picardie.fr

Eros Pasero
DET
Politecnico di Torino
Turin, Italy
eros.pasero@polito.it

***Abstract*—Continuous blood-pressure tracking is a key goal of healthcare AI, yet cuffs are still the norm in clinics and are unusable for this. We present a cuffless model that couples a Physics-Informed Neural Network (PINN) with basic hemodynamic laws to estimate full arterial pressure waveforms, from the aorta to the fingertip, using only an approximate inflow waveform Q(t) and a fingertip PPG and ECG signal. The network contains the Windkessel and 1-D Navier–Stokes models directly in its loss, so it learns realistic wave travel while needing no patient-specific calibration. Trained on records from the MIMIC-III Waveform Database, the network reproduces the expected changes in pulse shape along the arterial path. These results show that combining first-principles physics with deep learning could be a reliable, low-cost blood-pressure sensing.**

***Index Terms*—Blood pressure estimation, physics-informed neural networks, hemodynamics, cuffless monitoring, machine learning, electrocardiogram, photoplethysmogram, blood flow, ECG, PPG, ABP**

I. Introduction

Blood pressure (BP) is a basic marker of cardiovascular health, guiding the care of hypertension, heart failure, and vascular disease [1]. Cuff readings, though standard, are bulky and sporadic, so they miss short-term spikes and drops that matter in daily life [2]. Wearable, non-invasive monitors could close this gap and improve outcomes [3], yet today's methods still rely on calibration and struggle with the wide person-to-person spread in vascular properties [4].

BP changes with each patient's artery stiffness, blood volume, and cardiac output, so pure physics models such as the Windkessel approximation [5] are too coarse for bedside use [6]. Data-driven algorithms perform better but often ignore those same physical rules [7]. Physics-Informed Neural Networks (PINNs) promise a middle road: they blend first-principles constraints with the flexibility of deep learning, allowing the network to learn patient-specific pressure dynamics while respecting known hemodynamics [8].

By embedding cardiovascular physics into an AI model, this work advances healthcare AI toward continuous, cuff-free BP tracking: an essential step for safer, more personalised monitoring in everyday settings.

II. State of the Art

Cuff-less blood-pressure estimation from wearable ECG and PPG signals [9]–[11] has advanced rapidly, yet early models suffered from subject-specific variability, small training cohorts, and the lack of physiological constraints [12]. Recent work tackles these gaps in three complementary directions. First, physics-informed neural networks use cardiovascular equations directly into the loss, allowing accurate predictions with less ground-truth data [13]. Second, hybrid pipelines combine deep feature extraction and classical regression; a CNN + SVR cascade, for example, achieved mean absolute errors of 1.23 mmHg systolic and 3.08 mmHg diastolic, well inside the AAMI limits [14]. Third, operator-based and temporal architectures add richer priors: BP-DeepONet enforces Navier–Stokes dynamics and Windkessel boundaries [15], while a physics-informed temporal network augmented with adversarial contrastive learning captures the multi-periodic nature of BP and remains stable with few subject-specific samples [16].

Collectively, these approaches show that weaving physiological knowledge into modern machine-learning frameworks can curb overfitting and improve interpretability. Further gains, however, will hinge on broader datasets, stronger cross-population validation, and workflows that translate smoothly into clinical settings.

III. Challenges in Current Machine Learning Models for BP Prediction

Machine learning (ML) models for blood pressure (BP) estimation have achieved impressive performance metrics when trained and tested on the same dataset or patient group. However, when these models are applied to data from previously unseen patients or databases, they often fail to generalize effectively [17]. This limitation stems from several key issues inherent in both the data and the modeling approaches.

A. Morphology Over Physics

Neural networks trained on ECG and PPG inputs seems to excel at learning the morphological features of the signals rather than the underlying physical relationships between BP, ECG, and PPG. This is evident from the consistently high metrics reported when train, validation and test data are taken within the same database, expecially if windows are extracted without subject division. The networks, in these cases, learn to "recognize" the specific patterns associated with individual

patients' data rather than general principles that can apply universally.

When models fail on external datasets or new subjects, it suggests that the neural network has overfit to the individual characteristics of the training data, effectively discerning BP variations only for those specific patients. This highlights the critical need to transition from morphology-based learning to physics-informed modeling that respects the causal relationships between physiological signals and BP.

The use of ECG and PPG for blood pressure (BP) estimation faces several intrinsic challenges that arise from the physiological complexity of the circulatory system and the limitations of current modeling approaches. These challenges must be addressed to develop models capable of accurate and generalizable BP predictions. Below, we outline the key problems and considerations.

ECG and PPG traces carry each person's unique stamp because they depend on age, vessel health, body build, and day-to-day habits, making it hard to train one model that works for everyone [18]. Age-related changes in arterial stiffness and resistance shift the link between these signals and blood pressure, so any reliable model must allow for that [19].

ECG records the heart's electrical rhythm, not the mechanical pulse that drives blood pressure. The real trigger is the depolarisation phase that pushes flow Q_{in} into the arteries, as captured by the Windkessel view. When ECG is picked up far from the heart, for example at the fingertip, it becomes a distorted "phantom" version of the original signal, and both ECG and pressure waves drift over time, adding noise and lowering prediction accuracy.

To turn ECG into blood pressure we must track how the initial pulse BP_0 travels through elastic, branching vessels. Along the way the wave is damped, reflected, and reshaped by changing compliance and resistance [20]. Mapping ECG to the inflow Q_{in} that starts this wave is especially tricky when the ECG comes from peripheral sites [21].

PPG reacts directly to the pressure at the measurement point, so it gives a more immediate view of local BP than ECG. Yet it, too, is coloured by skin, tissue, and local vessel features, which complicates its use in global models [22].

Resistance and compliance shift with age, disease, and other personal factors [23]. Accurate BP estimates therefore need models that let these parameters vary. They must also respect the fluid-dynamic rules that govern how waves move and change; oversimplified shortcuts risk missing key behaviour [14].

IV. Proposed Solution

In this paper, we propose a novel framework that integrates hemodynamic, hydrodynamic, and wave evolution principles into a Physics-Informed Neural Network (PINN) to estimate ABP, using data from MIMIC III database [24]. The model is designed to eliminate the need for calibration and minimize dependency on subject-specific information, relying solely on PPG signals recorded from the fingertips and blood inflow Q_{in} approximation generated from ECG and PPG. This approach emphasizes user-friendliness while maintaining clinical accuracy and avoiding morphology learning by the network.

Our methodology leverages both physics-based and data-driven approaches to establish a robust, generalized link between Q_{in}, PPG, and BP. The key innovation lies in combining the physical principles of wave propagation and hemodynamics with neural network generalization capabilities to create a personalized yet scalable framework.

V. Blood Flow Rate Approximation

Photoplethysmography (PPG) can be interpreted, follwing Beer-Lambert law, as the reflected light intensity changes due to variations in blood volume through $PPG(t) = I_0 \cdot e^{-\mu(V_b(t)+V_t)}$ where $V_b(t)$ is the pulsatile blood volume in the tissue (variable over time) and V_t is the constant blood volume already prsent(non-pulsatile component).

The time derivative of the logarithm of the PPG signal, $\frac{d}{dt}\log PPG$, is directly related to the instantaneous rate of blood volume change.

To estimate the cardiac output Q_{in} without relying solely on ECG (which may suffer from morphological inconsistencies), we propose an approach utilizing PPG. Given that blood flow velocity is typically sharper near the proximal arteries ($x = 0$), we hypothesize that:

$$Q_{in}(t) \propto SV \cdot \frac{d}{dt}\log PPG \cdot \mathcal{F}(ECG), \tag{1}$$

where SV is the Stroke Volume and $\mathcal{F}(ECG)$ represents a frequency modulation function emphasizing QRS-related parts of the ECG. In our case we used a lowpass filter at 8 Hz cutoff frequency.

Furthermore, SV can be estimated as $SV \propto \max(PPG) - \min(PPG)$, as it corresponds to the integral of $\frac{d}{dt}\log PPG$ computed between systole and diastole. This formulation provides a direct approximation of stroke volume from PPG dynamics. In Fig.1 it is possible to see an example of generated Q_{in}.

VI. Database

The dataset used for this study is derived from the MIMIC-III Waveform Database, which contains high-resolution physiological signals, including ECG, PPG, and arterial blood pressure (ABP). The preprocessing pipeline ensures the integrity of the signals by filtering out segments with artifacts or missing data, ensuring a reliable basis for model training.

To approximate the cardiac inflow Q_{in}, we manually generate it using a combination of PPG and ECG signals, leveraging the previously described methodology. The data is segmented into overlapping windows of 1000 points, sampled at 125 Hz, corresponding to 8-second intervals of physiological activity. This windowing approach captures both local and global hemodynamic variations while maintaining computational efficiency.

After processing, a total of 156,000 valid windows were extracted, forming the dataset used for training and validation.

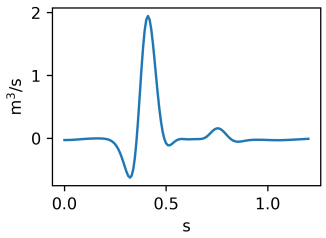


Fig. 1. Example of a waveform for the generated Q_{in}

This dataset formulation enables the training of a physics-informed neural network (PINN) that learns hemodynamic behavior while remaining independent of direct ABP measurements.

VII. Physics 1D Hemodynamics + Windkessel

To propagate the pressure wave from the aortic root to a distal site (e.g., the fingertip), we use the 1D hemodynamic PDEs, like [15]:

$$\frac{\partial A}{\partial t} + \frac{\partial Q}{\partial x} = 0, \quad \frac{\partial Q}{\partial t} + \frac{\partial}{\partial x}\left(\frac{Q^2}{A}\right) + \frac{A}{\rho}\frac{\partial p}{\partial x} = 0.$$

where Q(x,t) is the blood flow, A(x,t) is the sectional area of the blood vessel at x and P(x,t) is the blood pressure wave.

To close the system it was used a linear $p(A)$ relation:

$$p(x,t) = p_0 + \frac{\beta}{A_0}(A(x,t) - A_0).$$

A. Windkessel Model and Terminal Boundary Conditions

The terminal boundary condition at $x = L$ is enforced using the three-element Windkessel model, which approximates the vascular load downstream of the primary arterial segment. This model consists of a proximal resistance R_1, a compliance C, and a distal resistance R_2, forming an equivalent circuit for the pressure-flow relationship at the vascular outlet.

The governing equation for the Windkessel model is given by:

$$Q(L,t)\left(1 + \frac{R_1}{R2}\right) + CR_1\frac{dQ(L,t)}{dt} + \frac{p(L,t)}{R_2} - C\frac{dp(L,t)}{dt} = 0. \tag{2}$$

This equation ensures a physiologically meaningful representation of terminal reflections and compliance effects. The PINN framework incorporates this constraint as a penalty term in the loss function, ensuring that $p(L,t)$ remains consistent with downstream vascular dynamics.

B. PPG-Derived Pressure Approximation

To further refine the estimation of arterial blood pressure (ABP) at the distal site (e.g., fingertip), we introduce an empirical model linking PPG to pressure. Since PPG is a measure of volumetric changes in the microvasculature, we hypothesize a logarithmic relationship between PPG and local pressure $p(L,t) = p_0 + \alpha \log(\text{PPG}(t) + \epsilon)$, where p_0 represents the baseline pressure, α is a scaling coefficient capturing the sensitivity of pressure to volumetric changes, and ϵ is a small constant ensuring numerical stability.

C. Physiological Parameterization and Constraints

To keep the PINN within physiologically reasonable bounds, we introduce soft priors on a small set of well-established cardiovascular quantities: the blood density ($\rho \simeq 1060\ \text{kg m}^{-3}$), the local reference area $A_0(x)$, the pressure–area coupling $\beta(x)$, the distributed viscous resistance $K_r(x)$, and the Windkessel terminal elements (R_1, R_2, C), all expressed with respect to a baseline pressure p_0. By penalising departures from their usual clinical ranges rather than enforcing rigid values, the network is discouraged from drifting into non-physical regimes while still retaining enough freedom to adapt to patient-specific signatures.

D. Modeling of $A_0(x)$

The nominal vessel cross-sectional area $A_0(x)$ is modeled based on empirical arterial diameter distributions, following an exponential decay law $A_0(x) = \pi\left(\frac{d_0}{2}e^{-\lambda x}\right)^2$, where d_0 is the reference diameter at the aortic root (modeled like in Fig.2), and λ is a decay coefficient reflecting the tapering of the arterial tree. This formulation captures the gradual decrease in vessel diameter as blood flows toward the periphery.

E. Elasticity Parameter $\beta(x)$

The compliance coefficient $\beta(x)$ expresses how pressure deforms the vessel and can be written compactly as $\beta(x) = \sqrt{\pi}\,E(x)h_0(x)$, with $E(x)$ the local Young's modulus and $h_0(x)$ the wall thickness. Consistent with the treatment of $A_0(x)$, both quantities are assumed to follow exponential trends, namely $E(x) = E_0\,e^{\gamma x}$ and $h_0(x) = h_0^* e^{-\nu x}$. Using nominal values $E_0 = 0.77$ MPa, $h_0^* = 2.59$ mm, $\gamma = 1.49\ \text{m}^{-1}$ and $\nu = 2.06\ \text{m}^{-1}$, these soft priors encourage physiologically realistic vessel mechanics while still allowing the PINN to adapt to patient-specific data.

F. Modeling of the Resistance Parameter $K_r(x)$

Local viscous losses are captured by the resistance coefficient $K_r(x)$. Because plasma skimming and hematocrit redistribution make blood progressively thicker in the peripheral tree, we let the viscosity rise linearly from a baseline value $\mu_0 = 0.004\,\text{Pa}\cdot\text{s}$ to $\mu_{\max} = 0.006\,\text{Pa}\cdot\text{s}$ according to $\mu(x) = \mu_0 + (\mu_{\max} - \mu_0)x$. Inserting this profile into Poiseuille's scaling gives $K_r(x) = 8\pi\mu(x)/\rho$; resistance therefore grows with distance as viscosity increases, reproducing the heightened dissipation observed in smaller vessels.

VIII. PINN Structure, Losses, and Training

The proposed Physics-Informed Neural Network (PINN) integrates hemodynamic principles with deep learning, enabling a robust estimation of arterial blood pressure (ABP) using ECG and PPG signals. The model consists of three input branches: (i) a convolutional neural network (CNN) for $Q_{\text{in}}(t)$, (ii) a CNN for PPG, and (iii) a dense subnetwork for spatial coordinate x. These branches extract latent features and are subsequently combined to estimate hemodynamic parameters and pressure-flow evolution.

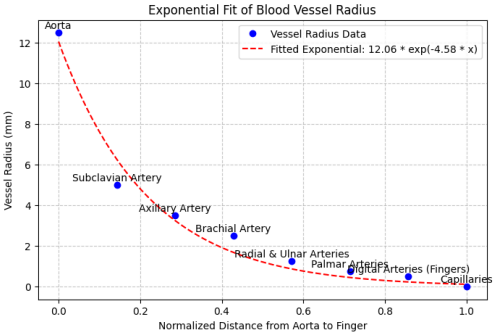


Fig. 2. Modeling d_0 from nominal physiological values find from general different sources online

A. Neural Network Architecture

a) Input Branches: The input space is composed of both temporal and spatial components essential for the model. Specifically, the inputs include 8 seconds (1000 timesteps) of the inflow rate $Q_{\text{in}}(t)$ and the photoplethysmogram signal $PPG(t)$, along with a spatial coordinate x within the normalized domain $[0, 1]$.

For each pair of $Q_{\text{in}}(t)$ and $PPG(t)$, spatial points x_n are uniformly sampled from the domain $[0, 1]$. The sampling process begins by randomly drawing N points from a uniform distribution. These sampled points are then sorted in ascending order to facilitate numerical differentiation and ensure accurate wave propagation modeling. To maintain stability in the learned dynamics, boundary points at $x = 0$ (representing the aorta and $x = 1$ (representing the distal site, such as the fingertip) are always included in the set of x_n points. Consequently, the network processes N inputs of the form (x_n, Q, PPG), where each x_n is paired with the same temporal signals $Q_{\text{in}}(t)$ and $PPG(t)$.

Both $Q_{\text{in}}(t)$ and $PPG(t)$ are individually passed through two consecutive residual convolutional blocks and skip connections. Each convolutional block consists of:

- 32 filters with a kernel size of 5,
- Batch normalization to stabilize and accelerate training,
- ReLU activation function to introduce non-linearity, and
- Dropout with a rate of 0.1 to enhance regularization and prevent overfitting.

The outputs from these convolutional blocks are then flattened and projected into a 32-dimensional latent space.

The spatial coordinate x is processed through the x-branch, which comprises two dense (fully connected) layers, each with 32 neurons, followed by dropout layers to improve generalization by preventing overfitting.

The features extracted from both the temporal and spatial branches are concatenated into a single feature vector. This combined feature vector is then fed into the learnable parameter estimation module, which is responsible for predicting the desired parameters based on the integrated temporal and spatial information.

b) Learnable Parameter Module: The PINN incorporates a learnable parameter layer that outputs physiologically constrained values for key arterial properties, including blood density ρ, arterial compliance β, nominal cross-sectional area A_0, and vascular resistance K_r. These parameters serve as soft constraints to guide the network toward physically meaningful solutions.

c) Prediction Layers: The final network layers integrate learned parameters with feature embeddings and propagate through fully connected layers (128 and 256 neurons), applying dropout (0.1) to prevent overfitting. So the outputs, at position X, for 8 seconds, are:

$$p(X,t) = f_\theta(X, Q_{\text{in}}, PPG), \quad Q(X,t) = g_\theta(X, Q_{\text{in}}, PPG), \tag{3}$$

where f_θ and g_θ represent the learned pressure and flow mappings.

B. Loss Functions

The training process is governed by a composite loss function combining data-driven and physics-based constraints:

$$\mathcal{L} = \lambda_{\text{PDE}}\mathcal{L}_{\text{PDE}} + \lambda_W\mathcal{L}_W + \lambda_{\text{ABP}}\mathcal{L}_{\text{ABP}} + \lambda_{\text{PPG}}\mathcal{L}_{\text{PPG}} + \lambda_{\text{reg}}\mathcal{L}_{\text{reg}}. \tag{4}$$

a) PDE Residual Loss.: Governs compliance with 1D hemodynamic equations:

$$\mathcal{L}_{\text{PDE}} = \left\| \frac{\partial A}{\partial t} + \frac{\partial Q}{\partial x} \right\|^2 + \left\| \frac{\partial Q}{\partial t} + \frac{\partial}{\partial x}\left(\frac{Q^2}{A}\right) + \frac{A}{\rho}\frac{\partial p}{\partial x} + K_r\frac{Q}{A} \right\|^2. \tag{5}$$

b) Windkessel Constraint.: Enforces terminal boundary conditions using a three-element Windkessel model:

$$\mathcal{L}_W = \left\| Q(L,t)R_1 + CR_1\frac{dQ(L,t)}{dt} - \frac{p(L,t)}{R_2} - C\frac{dp(L,t)}{dt} \right\|^2. \tag{6}$$

c) ABP Data Loss.: Ensures $p(x,t)$ follows available ABP measurements at the midpoint x_{mid}:

$$\mathcal{L}_{\text{ABP}} = \|p(x_{\text{mid}}, t) - \text{ABP}(t)\|^2. \tag{7}$$

d) PPG Constraint.: Constrains distal pressure estimation using a logarithmic PPG-pressure relation:

$$\mathcal{L}_{\text{PPG}} = \|p(L,t) - p_0 - \alpha\log(\text{PPG}(t) + \epsilon)\|^2. \tag{8}$$

e) Regularization Loss.: Enforces physiologically plausible constraints on estimated parameters:

$$\mathcal{L}_{\text{reg}} = \|\rho - \rho_0\|^2 + \left\|A_0 - A_0^{\text{nominal}}\right\|^2 + \left\|K_r - K_r^{\text{nominal}}\right\|^2. \tag{9}$$

The combination of these terms ensures accurate BP estimation while embedding domain knowledge into the network structure. The overall training objective minimizes $\mathcal{L}$ using the Adam optimizer with a learning rate of 10^{-3}, iterating over randomized spatial sampling for each training epoch.

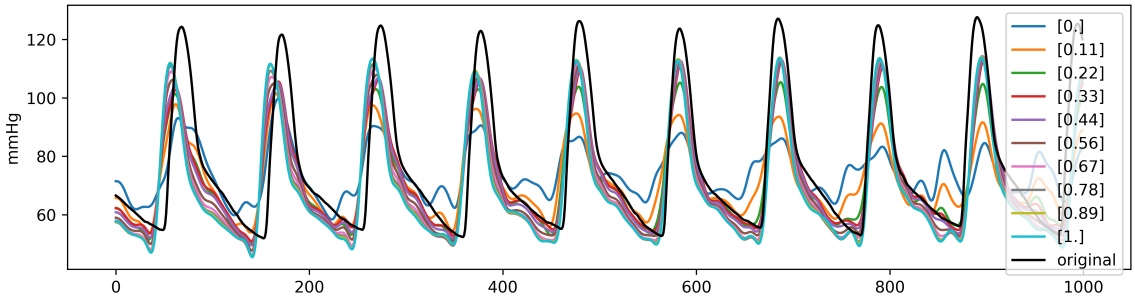


Fig. 3. ABP prediction for different values of x along the arm (from 0 to 1). On the X axis is timesteps (8 seconds). In black, the "ground truth" of the ABP.

IX. Training and Results

The network is trained on mini-batches of 16 wave pairs, each pair holding one signal of $Q_{\text{in}}(t)$ and PPG. Every pair is sampled at $N = 11$ points along the normalised vessel length $x \in [0, 1]$; one of those points is always the midpoint $x = 0.5$. A batch therefore supplies $16 \times 11 = 176$ input triplets $(x, Q_{\text{in}}, \text{PPG})$. We keep N small so that spatial derivatives stay stable and the losses enforced at $x = 0, 0.5, 1$ are not drowned out by the PDE residuals.

The dataset is split 80,%/10 %/10 % for training, validation and test. Fifty training epochs take about two hours on an NVIDIA RTX 3050.

A. Results and Observations

Figure 3 shows predicted arterial pressure from the aortic root ($x = 0$) to the fingertip ($x = 1$). The shapes follow well-known trends: the root wave has a wide systolic peak with reflections farther out, while the fingertip wave is sharper and displays stronger reflections. A small time shift appears between prediction and ground truth even though the records were peak-aligned, hinting that the network has learned the travel time of the pressure wave rather than merely copying the data.

X. Discussion and Conclusion

This preliminary work shows that a lightweight, physics-guided neural network can infer arterial blood pressure waveforms with physiologically coherent dynamics, even if the systolic peaks still need sharper reconstruction. The study therefore sets a baseline for calibration-free, patient-specific pressure estimation by blending data-driven fitting with cardiovascular laws.

Our next goal is to let the PINN adjust resistances $R_{1,2}$ and compliance C from simple anthropometric inputs (age, sex, height, weight) and to replace the heuristic cardiac inflow Q_{in} with a convolutional encoder–decoder that maps raw ECG + PPG directly to flow. These two upgrades—automatic parameter personalisation and a learnable inflow module—should yield a truly generalisable, clinically viable framework for non-invasive blood-pressure monitoring across diverse cohorts and settings.

Acknowledgment

Delrio acknowledges Eurecom for support in his PhD research.

References

[1] F. D. Fuchs and P. K. Whelton, "High blood pressure and cardiovascular disease," *Hypertension*, vol. 75, no. 2, pp. 285–292, 2020.

[2] N. Pilz, D. Picone, A. Patzak, O. Opatz, T. Lindner, L. Fesseler, V. Heinz, and T. Bothe, "Cuff-based blood pressure measurement: challenges and solutions," *Blood Pressure*, vol. 33, no. 1, p. 2402368, 2024.

[3] V. Bhaltadak, B. Ghewade, and S. Yelne, "A comprehensive review on advancements in wearable technologies: Revolutionizing cardiovascular medicine," *Cureus*, vol. 16, no. 5, 2024.

[4] R. Mukkamala, M. Yavarimanesh, K. Natarajan, J.-O. Hahn, K. G. Kyriakoulis, A. P. Avolio, and G. S. Stergiou, "Evaluation of the accuracy of cuffless blood pressure measurement devices: challenges and proposals," *Hypertension*, vol. 78, no. 5, pp. 1161–1167, 2021.

[5] N. Westerhof, J.-W. Lankhaar, and B. E. Westerhof, "The arterial windkessel," *Medical & biological engineering & computing*, vol. 47, no. 2, pp. 131–141, 2009.

[6] J. Flores-Gerónimo, A. Keramat, J. Alastruey, and Y. Zhang, "Uncertainty quantification of the pressure waveform using a windkessel model," *International journal for numerical methods in biomedical engineering*, vol. 40, no. 12, p. e3867, 2024.

[7] A. Arzani, J.-X. Wang, M. S. Sacks, and S. C. Shadden, "Machine learning for cardiovascular biomechanics modeling: challenges and beyond," *Annals of Biomedical Engineering*, vol. 50, no. 6, pp. 615–627, 2022.

[8] J. S. Shahoud, T. Sanvictores, and N. R. Aeddula, "Physiology, arterial pressure regulation," 2023.

[9] A. Paviglianiti, V. Randazzo, E. Pasero, and A. Vallan, "Noninvasive arterial blood pressure estimation using abpnet and vital-ecg," in *2020 IEEE International Instrumentation and Measurement Technology Conference (I2MTC)*, pp. 1–5, IEEE, 2020.

[10] V. Randazzo, P. Buccellato, J. Ferretti, F. Delrio, and E. Pasero, "Pulsecg-a cuffless non-invasive blood pressure monitoring device through neural network analysis of ecg and ppg signals," in *2024 IEEE 22nd Mediterranean Electrotechnical Conference (MELECON)*, pp. 1030–1035, IEEE, 2024.

[11] F. Delrio, V. Randazzo, G. Cirrincione, and E. Pasero, "Non-invasive arterial blood pressure estimation from electrocardiogram and photoplethysmography signals using a conv1d-bilstm neural network," *Engineering Proceedings*, vol. 39, no. 1, p. 78, 2023.

[12] S. B. Junaid, A. A. Imam, A. O. Balogun, L. C. De Silva, Y. A. Surakat, G. Kumar, M. Abdulkarim, A. N. Shuaibu, A. Garba, Y. Sahalu, *et al.*, "Recent advancements in emerging technologies for healthcare management systems: a survey," in *Healthcare*, vol. 10, p. 1940, MDPI, 2022.

[13] K. Sel, A. Mohammadi, R. I. Pettigrew, and R. Jafari, "Physics-informed neural networks for modeling physiological time series for cuffless blood pressure estimation," *npj Digital Medicine*, vol. 6, no. 1, p. 110, 2023.

[14] S. Rastegar, H. G. Hosseini, and A. Lowe, "Hybrid cnn-svr blood pressure estimation model using ecg and ppg signals," *Sensors*, vol. 23, no. 3, p. 1259, 2023.

[15] L. Li, X.-C. Tai, and R. Chan, "Bp-deeponet: A new method for cuffless blood pressure estimation using the physics-informed deeponet," *arXiv preprint arXiv:2402.18886*, 2024.
[16] R. Wang *et al.*, "Adversarial contrastive learning based physics-informed temporal networks for cuffless blood pressure estimation," *arXiv preprint arXiv:2408.08488*, 2024.
[17] C. Aguet, J. Van Zaen, M. Proença, G. Bonnier, P. Frossard, and M. Lemay, "Generalization capability of a neural network for blood pressure estimation from photoplethysmography," in *2022 Computing in Cardiology (CinC)*, vol. 498, pp. 1–4, IEEE, 2022.
[18] G. Chen, L. Zou, and Z. Ji, "A review: Blood pressure monitoring based on ppg and circadian rhythm," *APL bioengineering*, vol. 8, no. 3, 2024.
[19] P. H. Charlton, B. Paliakaitė, K. Pilt, M. Bachler, S. Zanelli, D. Kulin, J. Allen, M. Hallab, E. Bianchini, C. C. Mayer, *et al.*, "Assessing hemodynamics from the photoplethysmogram to gain insights into vascular age: a review from vascagenet," *American Journal of Physiology-Heart and Circulatory Physiology*, vol. 322, no. 4, pp. H493–H522, 2022.
[20] G. M. London and A. P. Guerin, "Influence of arterial pulse and reflected waves on blood pressure and cardiac function," *American heart journal*, vol. 138, no. 3, pp. S220–S224, 1999.
[21] M. E. Safar and H. S. Boudier, "Vascular development, pulse pressure, and the mechanisms of hypertension," *Hypertension*, vol. 46, no. 1, pp. 205–209, 2005.
[22] J. Park, H. S. Seok, S.-S. Kim, and H. Shin, "Photoplethysmogram analysis and applications: an integrative review," *Frontiers in Physiology*, vol. 12, p. 808451, 2022.
[23] G. E. McVeigh, C. W. Bratteli, D. J. Morgan, C. M. Alinder, S. P. Glasser, S. M. Finkelstein, and J. N. Cohn, "Age-related abnormalities in arterial compliance identified by pressure pulse contour analysis: aging and arterial compliance," *Hypertension*, vol. 33, no. 6, pp. 1392–1398, 1999.
[24] A. Johnson, T. Pollard, and R. Mark, "MIMIC-III clinical database."